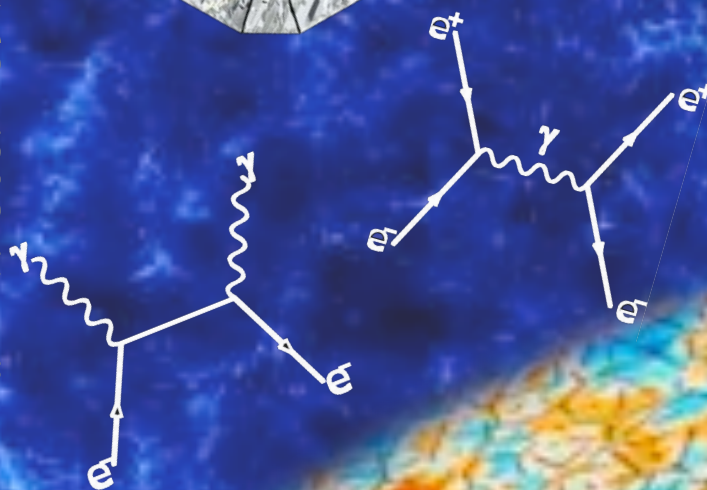
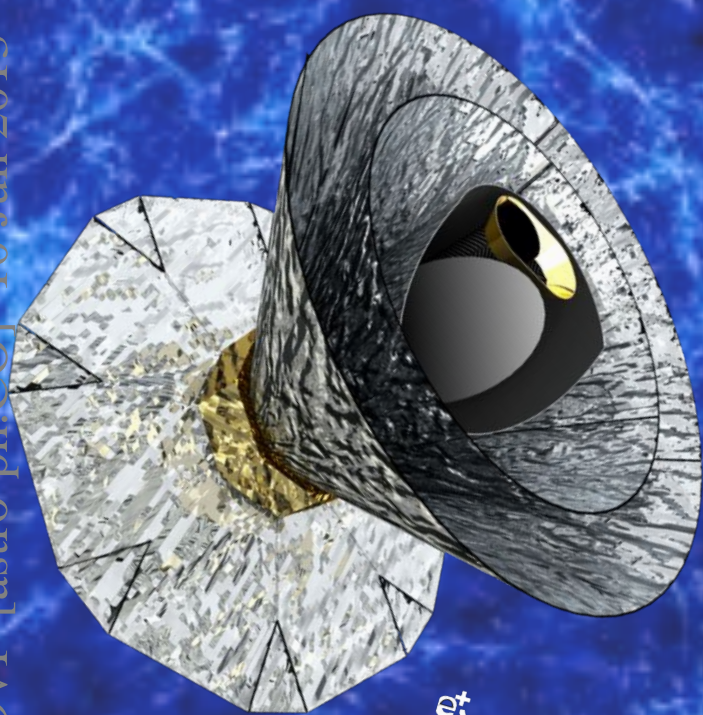


**Polarized Radiation Imaging and Spectroscopy Mission**

# **PRISM**

**Probing cosmic structures and radiation  
with the ultimate polarimetric spectro-imaging  
of the microwave and far-infrared sky**

arXiv:1306.2259v1 [astro-ph.CO] 10 Jun 2013



**Spokesperson: Paolo de Bernardis**  
e-mail: [paolo.debernardis@roma1.infn.it](mailto:paolo.debernardis@roma1.infn.it) — tel: + 39 064 991 4271

## Authors and contributors

Philippe André, Carlo Baccigalupi, Domingos Barbosa, James Bartlett, Nicola Bartolo, Elia Battistelli, Richard Battye, George Bendo, Jean-Philippe Bernard, Marco Bersanelli, Matthieu Béthermin, Pawel Bielewicz, Anna Bonaldi, François Bouchet, François Boulanger, Jan Brand, Martin Bucher, Carlo Burigana, Zhen-Yi Cai, Viviana Casasola, Guillaume Castex, Anthony Challinor, Jens Chluba, Sergio Colafrancesco, Francesco Cuttaia, Giuseppe D'Alessandro, Richard Davis, Miguel de Avillez, Paolo de Bernardis, Marco de Petris, Adriano de Rosa, Gianfranco de Zotti, Jacques Delabrouille, Clive Dickinson, Jose Maria Diego, Edith Falgarone, Pedro Ferreira, Katia Ferrière, Fabio Finelli, Andrew Fletcher, Gary Fuller, Silvia Galli, Ken Ganga, Juan García-Bellido, Adnan Ghribi, Joaquin Gonzalez-Nuevo, Keith Grainge, Alessandro Gruppuso, Alex Hall, Carlos Hernandez-Monteagudo, Mark Jackson, Andrew Jaffe, Rishi Khatri, Luca Lamagna, Massimiliano Lattanzi, Paddy Leahy, Michele Liguori, Elisabetta Liuzzo, Marcos Lopez-Caniego, Juan Macias-Perez, Bruno Maffei, Davide Maino, Silvia Masi, Anna Mangilli, Marcella Massardi, Sabino Matarrese, Alessandro Melchiorri, Jean-Baptiste Melin, Aniello Mennella, Arturo Mignano, Marc-Antoine Miville-Deschênes, Federico Nati, Paolo Natoli, Mattia Negrello, Fabio Noviello, Francesco Paci, Rosita Paladino, Daniela Paoletti, Francesca Perrotta, Francesco Piacentini, Michel Piat, Lucio Piccirillo, Giampaolo Pisano, Gianluca Polenta, Sara Ricciardi, Matthieu Roman, Jose-Alberto Rubino-Martin, Maria Salatino, Alessandro Schillaci, Paul Shellard, Joseph Silk, Radek Stompor, Rashid Sunyaev, Andrea Tartari, Luca Terenzi, Luigi Toffolatti, Maurizio Tomasi, Tiziana Trombetti, Marco Tucci, Bartjan Van Tent, Licia Verde, Ben Wandelt, Stafford Withington

## Coordination group

*The preparation of this science case submitted to ESA has been coordinated by:*

James Bartlett, François Bouchet, François Boulanger, Martin Bucher, Anthony Challinor, Jens Chluba, Paolo de Bernardis (spokesperson), Gianfranco de Zotti, Jacques Delabrouille (coordinator), Pedro Ferreira, Bruno Maffei

## Supporters

As a result of the highly successful ESA Planck and Herschel missions, Europe has acquired considerable scientific and technical expertise in the scientifically fruitful and strategic field of microwave and far-infrared observations and trained a new generation of young European astronomers in this area. The science themes outlined in this proposal are the logical next step that will allow ESA to capitalize on these strengths.

To demonstrate the breadth of support for PRISM, we are in the process of assembling a list of supporters that can be found at the following website:

<http://www.prism-mission.org>

Scientists who believe that ESA should pursue as part of its programme the science themes presented in this White Paper are strongly encouraged to visit the website and to sign on as supporters.

## PRISM Steering committee

**France:** François Bouchet, Martin Bucher, Jacques Delabrouille, Martin Giard

**Germany:** Jens Chluba, Rashid Sunyaev

**Ireland:** Anthony Murphy

**Italy:** Marco Bersanelli, Carlo Burigana, Paolo de Bernardis

**Netherlands:** Rien van de Weijgaert

**Portugal:** Carlos Martins

**Spain:** Enrique Martínez-González, José Alberto Rubiño-Martín, Licia Verde

**Switzerland:** Martin Kunz

**United Kingdom:** Anthony Challinor, Joanna Dunkley, Bruno Maffei

---

This is a corrected version (10 June 2013) of the original document submitted on 24 May 2013 to ESA in response to *Call for White Papers for the definition of the L2 and L3 Missions in the ESA Science Programme* (<http://sci.esa.int/Call-WP-L2L3>)

# 1 Executive summary

*PRISM* is a large-class mission that will carry out the ultimate survey of the microwave to far-infrared sky in both intensity and polarization as well as measure its absolute spectrum. *PRISM* will consist of two instruments: (1) a high angular resolution polarimetric imager with a 3.5 m telescope cooled to around 4K to reduce thermal noise, particularly in the far-infrared bands; and (2) a low angular resolution spectrometer to compare the sky frequency spectrum to a nearly perfect reference blackbody. The two instruments working in tandem will enable *PRISM* to make breakthrough contributions by answering key questions in many diverse areas of astrophysics and fundamental science. A few highlights of the new science with *PRISM* include:

**(A) The ultimate galaxy cluster survey:** The Sunyaev-Zeldovich (SZ) effect is the method of choice for assembling a catalog of clusters at high redshift, of particular interest for cosmology because of the tight correlation between integrated  $y$ -distortion and cluster mass. When *PRISM* flies, all-sky cluster samples (e.g., from *eROSITA*, *Euclid*) will likely count some  $10^5$  objects, mostly at  $z < 1$ . *PRISM* will find 10 times more clusters extending to deeper redshifts, with many thousands beyond  $z = 2$ . In fact, *PRISM* will detect all clusters in the universe of mass larger than  $10^{14}M_{\odot}$ , and a large fraction of those with mass above  $5 \times 10^{13}M_{\odot}$ . Owing to its exquisite spectral coverage, angular resolution and sensitivity, *PRISM* will measure the peculiar velocity of hundreds of thousands of clusters using the kinetic SZ effect, initiating a new research area: the complete mapping of the large-scale velocity field throughout our Hubble volume. In addition, *PRISM* will also be able to probe the relativistic corrections to the classic SZ spectral distortion spectrum, thus measuring the gas temperature. This cluster sample will allow us to probe dark energy and better understand structure formation at large redshift.

**(B) Understanding the Cosmic Infrared Background:** Most star formation in the universe took place at high redshift. Hidden from optical observations by shrouds of dust in distant galaxies, it is visible only in the far infrared or in X-rays. Emission from these dusty galaxies constitutes the cosmic infrared background (CIB) which *PRISM*, owing to its high sensitivity and angular resolution in the far infrared, is uniquely situated to investigate. The survey will sharpen and extend to higher redshifts the determination of the bolometric luminosity function and the clustering properties of star-forming galaxies. Tens of thousands of easily recognizable, bright, strongly lensed galaxies and hundreds of the very rare maximum starburst galaxies, up to  $z > 6$ , will be detected, providing unique information on the history of star formation, the physics of the interstellar medium in a variety of conditions up to the most extreme, and the growth of large scale structure, including proto-clusters of star-forming galaxies. The survey will also probe the evolution of radio sources at (sub-)mm wavelengths and provide measurements of the spectral energy distribution (SED) of many thousands of radio sources over a poorly explored, but crucial frequency range.

**(C) Detecting inflationary gravity waves:** Present precision measurements of cosmic microwave background (CMB) temperature anisotropies lend considerable support to simple models of inflation. However the most spectacular prediction of inflation—the generation of gravitational waves with wavelengths as large as our present horizon—remains unconfirmed. Several initiatives from the ground and from stratospheric balloons are currently underway to attempt to detect these gravitational waves through the B-mode spectrum of the CMB polarization. However, they suffer from severe handicaps such as limited frequency coverage due to atmospheric opacity, unstable seeing conditions, and far sidelobes from the ground. It is only from space that one may hope to detect the very low- $\ell$  B-modes due to the re-ionization bump. Because of its broad frequency coverage and extreme stability, *PRISM* will be able to detect B-modes at  $5\sigma$  for  $r = 5 \times 10^{-4}$ , even under pessimistic assumptions concerning the complexity of the astrophysical foreground emissions that must be reliably removed. Moreover, *PRISM* will be able to separate and filter out the majority of the lensing signal due to gravitational deflections.

**(D) Probe new physics through CMB spectral distortions:** The excellent agreement between the microwave sky emission and a perfect blackbody observed by the *COBE FIRAS* instrument is rightfully highlighted as a crucial confirmation of Big Bang cosmology. However theory predicts that at higher sensitivity this agreement breaks down. Some of the predicted deviations are nearly sure bets. Others provide powerful probes of possible new physics. The *PRISM* absolute spectrometer will measure the spectrum more than three orders of magnitude better than *FIRAS*.  $y$ -distortions from the re-ionized gas as well as from hot clusters constitute a certain detection. However  $\mu$ -distortions and more general spectral distortions have the potential to uncover decaying dark matter and to probe the primordial power spectrum on very small scales that cannot be measured by other means, being contaminated by the nonlinearity of gravitational clustering at late times.

**(E) Probe Galactic astrophysics:** *PRISM* will have a major impact on Galactic astrophysics by providing a unique set of all-sky maps. *PRISM* will extend Herschel dust observations to the whole sky and will map emission lines key to quantifying physical processes. The survey will have the sensitivity and angular resolution required to map dust polarization down to sub-arcminute resolution even at the Galactic poles. No project will provide a comparable perspective on interstellar components over such a wide range of scales. The *PRISM* data will provide unique clues to study the interstellar medium, the Galactic magnetic field, and star formation, and will address three fundamental questions in Galactic astrophysics: What are the processes that structure the interstellar medium? What role does the magnetic field play in star formation? What are the processes that determine the composition and evolution of interstellar dust?

These are but a few of the highlights of the rich and diverse physics and astrophysics that *PRISM* will be able to carry out.

## 2 Legacy archive

The hundreds of intensity and polarization maps of *PRISM* will constitute a legacy archive useful for almost all branches of astronomy for decades to come. Combining low resolution spectrometer data and high resolution images from the imager, *PRISM* will deliver a full spectro-polarimetric survey of the full sky from  $50\ \mu\text{m}$  to  $1\ \text{cm}$ . The spectral resolution will range from about  $0.5\ \text{GHz}$  to  $15\ \text{GHz}$  at  $1.4^\circ$  angular resolution, and from  $\delta\nu/\nu \approx 0.025$  to  $0.25$  at the diffraction limit of a  $3.5\ \text{m}$  telescope (from  $\sim 6''$  to  $17'$ ).

We will make public full-sky maps of the absolute temperature of the CMB and of its polarization (at a resolution of about 2 arcminutes with a sensitivity of order  $1\ \mu\text{K}$  or better per resolution element), of the emission of all galactic components in absolute intensity and polarization (including main spectral lines), and several catalogues of various galactic and extragalactic objects, among which a catalogue of about a million galaxy clusters and large groups up to redshift  $z = 3$  or more.

## 3 Probing the Universe with galaxy clusters

The *PRISM* mission will exploit the advantages of cluster surveying using the SZ effect in a spectacular way, surpassing in depth any planned cluster survey and, in addition, achieving an objective unattainable in any other way: measurement of the cosmic velocity field throughout the observable universe. In short, we will detect cluster and group systems throughout our Hubble volume from the moment when they first emerge. *PRISM* will also provide cluster mass determinations out to high redshift through gravitational lensing of the CMB in both temperature [96] and polarization [66], something only possible because of *PRISM*'s high angular resolution and frequency coverage extending into bands unreachable from the ground. The *Planck*, ACT, and SPT experiments demonstrated the potential of the Sunyaev-Zeldovich effect for studying galaxy clusters and using them to constrain cosmological models. *PRISM* will transform SZ cluster studies into arguably our most powerful probe of cosmic large-scale structure and its evolution.

**The Cluster Catalog and its Applications:** We estimate the content of the *PRISM* SZ catalog by applying a multi-frequency matched filter [70] to simulations of a typical field at intermediate Galactic latitude. Our detection mass remains below  $10^{14}$  solar masses at *all redshifts* (Fig. 1). Extrapolating from the observed *Planck* counts, we predict nearly  $10^6$  clusters with many thousands at  $z > 2$ . We already know from *Planck* SZ observations [79, 80] that the SZ signal in clusters scales as our adopted relation down to much smaller masses in the local universe, leaving as our main uncertainty poor knowledge of its redshift dependence. This is, of course, the primary motivation for studying the high redshift cluster population.

Based on this calculation, *PRISM* will surpass all current and planned cluster surveys, including *eROSITA* and *Euclid*—not just in total numbers, but most importantly in numbers of objects at  $z > 1.5$ . Cluster

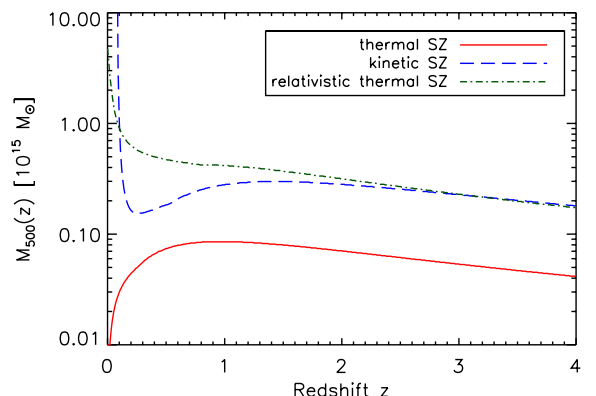


Figure 1: Lower mass limits for detection of the indicated SZ effects at signal-to-noise  $S/N > 5$  as a function of redshift.

identification will be vastly more robust for *PRISM* than Euclid, which will suffer from the much higher contamination rate of optical/NIR cluster searches, especially at redshifts beyond unity. In all cases, only *PRISM* has the ability to find significant numbers of clusters in the range  $2 < z < 3$ , the critical epoch that current observations identify as the emergence of the characteristic cluster galaxy population on the red sequence. *PRISM* will also enable us to explore the abundance of the intra-cluster medium (ICM) through the  $Y-M$  relation and its relation to the galaxy population at these high redshifts.

At the time of operation, large imaging (e.g., *DES*, *LSST*, *HSC*) and spectroscopic surveys (e.g., *4MOST*, *PFS*, *WEAVE*, *BigBOSS/MS-DESI*, *SKA*) will have covered the entire extragalactic sky. We will easily be able to obtain redshifts, spectroscopic or photometric, for all objects to  $z = 2$ , and the two micron cutoff of Euclid’s IR photometric survey (H band) will be sufficient to detect the  $4000\text{\AA}$  break in brighter cluster galaxies at higher redshifts.

**Catalog as a cosmological probe:** As an example of the cosmology constraints that can be obtained from the expected cluster catalog, we performed a standard Fisher analysis to constrain four parameters,  $\Omega_m$ ,  $\sigma_8$  and the dark energy equation-of-state parameters  $w_0$  and  $w_1$ , in a standard flat  $\Lambda$ CDM cosmological model. The constraints on the latter dark energy parameters are  $w_0 = -1 \pm 0.003$  and  $w_1 = 0 \pm 0.1$  after marginalization over the first two parameters. Despite its simplicity, this example nevertheless illustrates the power of the *PRISM* cluster catalog as a dark energy probe.

**Cosmic velocity field:** *PRISM* will initiate an untapped research area: study of the velocity field through the kinetic SZ effect [102, 90, 8], an independent probe of dark matter and large-scale structure evolution. In Fig. 1 we show mass limit to which we expect to measure a velocity of  $300 \text{ km s}^{-1}$  to five sigma on individual clusters. This mass limit means that we will obtain velocity measurements for hundreds of thousands of clusters out to the highest redshifts. In addition, by comparing measured velocities to mass concentrations, say from Euclid lensing or galaxy surveys, we can test the theory of gravity on cosmic scales and to high redshift. This science is unattainable by any other means.

**Relativistic and non-thermal effects:** We will determine the temperature of clusters down to a mass limit just above  $10^{14}$  solar masses by measuring the relativistic corrections to the thermal SZ spectrum [89, 15, 55, 95, 8]. These same characteristics allow us to search for non-thermal signatures in the spectra that could signal the presence of highly energetic particles, perhaps dark matter annihilation products, and even study the temperature structure of the most massive systems.

**Diffuse SZ and the cosmic web:** The diffuse, unresolved SZ effect probes a different mass and redshift range than observations of individually detected objects. We will study this diffuse effect through the power spectrum and higher order moments of an SZ map of the sky. *Planck* recently extracted the first Compton parameter ( $y$ -fluctuation) map [85], but the results are limited by foregrounds and noise. With many more spectral bands and much better sensitivity and resolution, *PRISM* will significantly improve the results, making possible attempts to directly map the cosmic web (i.e., its filaments) over large scales through its diffuse gas content.

We will explore the gas content of dark matter halos down to very low masses, a research area pioneered by *Planck* by stacking SZ measurements based on known objects to detect the signal down below  $10^{13}$  solar masses [79, 80]. The measurement over such a vast range is unique to the SZ effect and a highly valuable constraint on the mysteries of the feedback mechanisms at the heart of galaxy formation. *PRISM* greatly expands this important science area by pushing to the lowest possible masses and by probing gas content as a function of object properties. Coupled with our lensing measurements, we have a new and exceptional tool to study the relation between luminous and dark matter.

**Polarized SZ effect:** *PRISM* will enable searches for the polarized SZ effects, giving access to transverse cluster velocities and measurements of the CMB quadrupole at distant locations.

## 4 Extragalactic sources and the cosmic infrared background

**Early evolution of galaxies:** Although *Herschel* and *Spitzer* made spectacular advances in our understanding of early, dust enshrouded phases of galaxy evolution, our knowledge of star-formation history in the distant universe is still very incomplete. The *PRISM* mission will make essential progress thanks to its unique properties: full sky coverage and unparalleled frequency range. As illustrated in Fig. 2, *PRISM*’s unprecedented frequency coverage provides direct measurements of the bolometric luminosities of star-forming galaxies up to high redshifts. At  $z \gtrsim 2$ , i.e., in the redshift range where both the cosmic star formation and

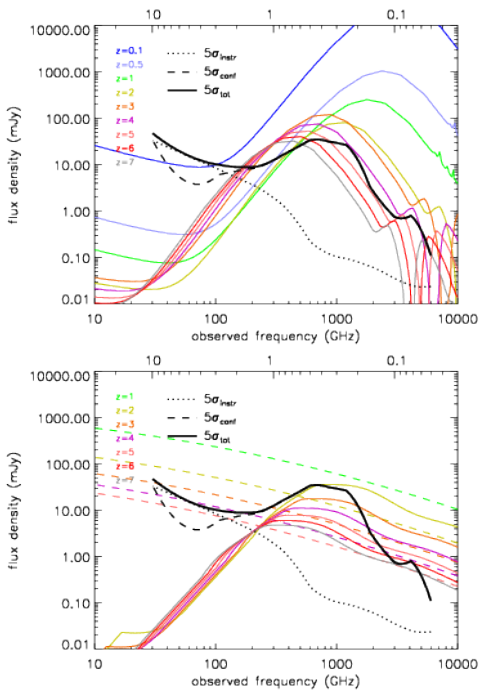


Figure 2: SEDs of dusty galaxies (top panel) and of AGNs (bottom panel) at different redshifts compared with estimated  $5\sigma$  detection limits (solid black line) taking into account instrumental and confusion noise summed in quadrature. The instrumental noise refers to the full mission. The  $5\sigma$  detection limits allowing for either component are shown by the dotted and the dashed black lines, showing that *PRISM* is confusion limited above  $\approx 150$  GHz. We have assumed that component separation techniques, extensively validated both on simulations and on real data, can efficiently remove diffuse emissions such as the CMB (that would otherwise dominate the fluctuation field for  $\nu \lesssim 220$  GHz) and Galactic emissions. In the top panel, at  $z = 0.1$  and  $0.5$  we have plotted the Arp 220 SED scaled to an IR (8–1000  $\mu\text{m}$ ) luminosity of  $10^{12} L_{\odot}$ . At  $z \geq 1$  we have used the SED of the  $z \approx 2.3$  galaxy SMM J2135-0102 scaled to  $L_{\text{IR}} = 10^{13} L_{\odot}$  for  $z = 1$  and  $z = 2$ , and to  $L_{\text{IR}} = 3 \cdot 10^{13} L_{\odot}$  [the luminosity of the  $z = 6.34$  galaxy detected by *Herschel*/SPIRE, 91] for  $z \geq 3$ . In the bottom panel, the solid colored lines represent SEDs of a type-2 QSO (contribution of the host-galaxy subtracted) with  $L_{\text{IR}} = 10^{13} L_{\odot}$  at several redshifts  $\geq 2$ , while the dashed colored lines show a schematic representation of the SED of the prototype blazar 3C 273 shifted to redshifts from 1 to 5.

the accretion rate onto supermassive black-holes are maximum, both the IR peak associated with the dusty torus around AGN ( $\lambda_{\text{p,AGN}} \approx 30 \times (1+z) \mu\text{m}$ ) and the peak of dust emission in the host galaxy are within the covered range. Moreover, measurements of the complete far-IR to mm-wave SED will vastly improve the accuracy of photometric redshift estimates that have a rms error of  $\approx 0.2(1+z)$  with SPIRE alone [65]. This means that the *PRISM* survey will allow us to characterize to high statistical precision the evolution with redshift of the bolometric luminosity function. At  $z \gtrsim 2$  it will be possible to investigate the relationships between star-formation and nuclear activity: What fraction of the bolometric energy radiated by star-forming galaxies is produced by accretion onto supermassive black holes in active galactic nuclei (AGN)? What are the evolution properties of far-IR selected AGNs? What fraction of them is associated with active star formation? Are the growth of central super-massive black hole formation and the build-up of stellar populations coeval? The substantially higher spatial resolution (thanks to the shorter wavelength channels) and the correspondingly higher positional accuracy compared to *Herschel*/SPIRE will greatly improve identification of reliable counterparts in other wavebands, necessary for a comprehensive understanding of the properties of detected galaxies.

Its all-sky coverage makes *PRISM* uniquely suited to study rare phenomena. Examples are the ‘maximum starburst’ galaxy at  $z = 6.34$ , detected by *Herschel*/SPIRE [91], or the most luminous star-forming hyper-luminous IR galaxies, such as the binary one, pinpointing a cluster of star-bursting proto-ellipticals at  $z = 2.41$  discovered by Ivison et al. [56]. The  $z = 6.34$  galaxy was found when looking for *ultra-red* sources with flux densities  $S_{250\mu\text{m}} < S_{350\mu\text{m}} < S_{500\mu\text{m}}$ . The *PRISM* survey will allow us to look for even redder sources, potentially at even higher redshifts, and will provide a test of our understanding of the interstellar medium and of star-formation under extreme conditions.

Strongly gravitationally lensed systems have long been very difficult to identify in sufficiently large numbers to be statistically useful. This situation changed drastically with the advent of (sub-)mm surveys. One of the most exciting *Herschel*/SPIRE results was the direct observational confirmation that almost all the galaxies brighter than  $\approx 100$  mJy at  $500 \mu\text{m}$  are either strongly lensed or easily identifiable low- $z$  spirals [72]. The surface density of strongly lensed high- $z$  galaxies above this limit is  $\approx 0.3 \text{ deg}^{-2}$ , implying that an all-sky survey can detect  $\sim 10^4$  such systems. The fact that these sources are very bright makes redshift measurements with CO spectrometers and high resolution imaging with millimeter interferometers relatively easy. This will allow us to get detailed information on obscured star formation in the early Universe and the on processes driving it in observing times hundreds of times shorter than would be possible without the help of gravitational amplification and with an effective source-plane resolution several times higher than could otherwise be achieved.

Large numbers of strongly lensed galaxies are also expected from large area optical surveys. It should be noted, however, that sub-mm selection has important distinctive properties. The selected lensed galaxies are very faint in the optical, while most foreground lenses are passive ellipticals, essentially invisible at sub-mm wavelengths so that there is no, or little, contamination between images of the source and of the lens. This

makes possible the detection of lensing events with small impact parameters. Also, compared to the optical selection, (sub-)mm selection allows us to probe earlier phases of galaxy evolution.

Optical spectroscopy of galaxies acting as lenses can be exploited to measure the mass distribution of their dark matter halos as a function of redshift. Note that *Euclid* will directly provide redshifts for the majority of the lenses out to  $z \sim 1$  in its area. The large number of newly identified strongly lensed galaxies will directly probe the evolution of large-scale structure. Large samples of strongly lensed galaxies are also essential for many other astrophysical and cosmological applications [106].

*PRISM* will study the angular correlation function of detected sources with much better statistics than was possible with *Herschel*'s extragalactic surveys that, altogether, cover little more than 2% of the sky. Also, the accurate photometric redshifts will allow us to follow evolution with cosmic time. Clustering properties measure the mass of dark matter halos associated with galaxies and are a powerful discriminant for galaxy formation and evolution models. Studies of the correlation function of the power spectrum also establish occupation numbers of star-forming galaxies, and therefore their environments. In particular this study will allow us to detect high- $z$  *proto-clusters* of dusty galaxies. We thus investigate an earlier evolutionary phase of the most massive virialized structures in the Universe. This science is possible only in the wavebands covered by *PRISM*.

The *PRISM* clustering data will extend to much higher redshift than *Euclid*, whose wide-area survey will accurately map the galaxy distribution up to  $z \sim 1$ . The *PRISM* data will provide information at higher  $z$ , and primarily over the redshift range  $2 < z < 3$ , corresponding to the peak in star formation activity. Moreover, optical and near-IR data severely underestimate the SFR of dust obscured starbursts and may entirely miss these objects, which are the main targets of far-IR/sub-mm surveys such as *PRISM*. Only the combination of *PRISM* and *Euclid* data will provide a complete view of the spatial distribution of galaxies and of how star formation is distributed among dark matter halos.

The *PRISM* sensitivity and spectral coverage will allow substantially improved measurements of the cosmic infrared background (CIB) spectrum with an accurate removal of all contaminating signals. *PRISM* will also measure in a uniform way the CIB power spectrum over an unprecedented range of frequencies and of angular scales (from  $\sim 10$  arcsec to tens of degrees).

**Radio sources:** *PRISM* will extend the counts of radio sources, both in total and in polarized intensity, by at least one order of magnitude downwards in flux density compared to *Planck*. Above 217 GHz, the counts will be determined for the first time over a substantial flux density range with good statistics. This will make possible the first investigation of the evolutionary properties of radio sources at (sub-)mm wavelengths. *PRISM* will provide measurements of the spectral energy distribution (SED) of many thousands of radio sources and of multifrequency polarization properties for hundreds of them. The vast majority of these sources are expected to be blazars, and the accurate determination of their spectra will allow us to understand how physical processes occurring along relativistic jets shape the SED. For steep-spectrum sources we will obtain the distribution of break frequencies due to electron aging, allowing an unbiased estimate of the distribution of radio source ages. Moreover, these observations will shed light on the relationship between nuclear radio emission and star formation activity in the host galaxies.

## 5 Inflation and CMB primordial B-modes

At the heart of modern cosmology is a set of initial conditions generated at very early times by what is known as *cosmic inflation*. During inflation, the Universe undergoes a period of ultra-rapid accelerated expansion, typically driven by a fundamental scalar field  $\phi$ , with a potential energy  $V(\phi)$  that dominates over its kinetic energy. Quantum fluctuations of spacetime and the scalar field are amplified and stretched to cosmological scales resulting in a quasi-Gaussian stochastic distribution of density perturbations with amplitude  $A_S$ , and a scale dependence characterized by the *scalar spectral index*,  $n_S \equiv 1 + d \ln A_S^2(k) / d \ln k$ . Theory predicts that  $A_S$  and  $n_S$  depend on the details of  $V$  and hence  $\phi$ . Furthermore, interactions of  $\phi$  with itself and with other fields induce cross-correlations between perturbation modes, leading to non-Gaussianity which can be detected in higher order statistics (bispectrum, trispectrum). Inflation also produces a bath of primordial gravitational waves characterized by an amplitude  $A_T$  and the tensor spectral index  $n_T = d \ln A_T^2(k) / d \ln k$ . Remarkably, in the simplest models of inflation, the ratio between the tensor and scalar perturbations,  $r$ , is a direct probe of  $V$  in the early Universe:  $r \equiv 16(A_T/A_S)^2 \approx M_{Pl}^2(V'/V)^2$ . Present observations estimate that  $V^{1/4} = 3.3 \times 10^{16} r^{1/4}$  GeV, so that measuring  $r$  effectively translates into a measurement of the energy scale of inflation. A measurement of  $r$ ,  $n_S$ , and  $n_T$  can directly probe the physics of the early Universe for which

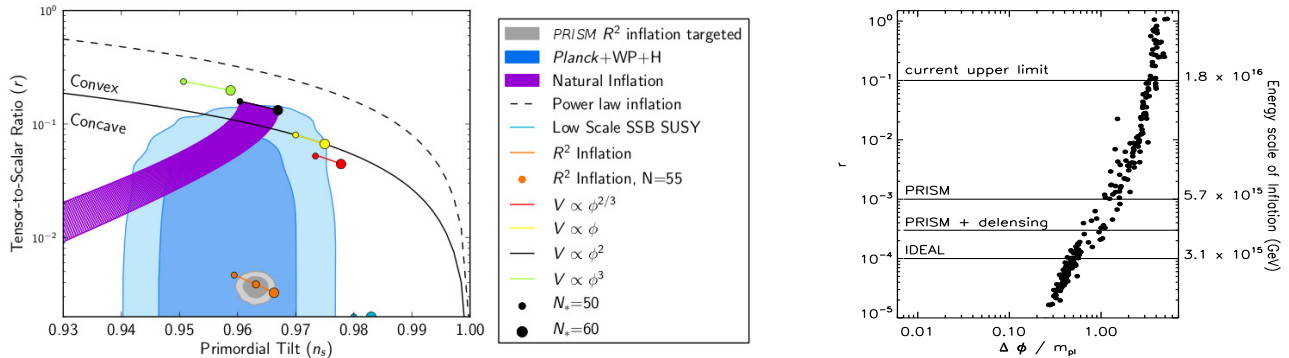


Figure 3: Left: Constraints on inflationary potentials from *Planck* and the predicted constraints from *PRISM* (not assuming de-lensing) for a fiducial value of  $r = 5 \times 10^{-2}$  (adapted from [86]). Right: distribution of inflationary model parameters generated using a model independent approach that Monte-Carlo samples the inflationary flow equations. While these simulations cannot be interpreted in a statistical way (e.g., Kinney [63], Peiris et al. [77], Chongchitnan and Efstathiou [26]), they show that models cluster around attractor regions (adapted from [107]).

there is a very rich phenomenology. Single field inflation models can relate  $r$  directly with the evolution of  $\phi$  at early times. Indeed, for an inflationary expansion lasting long enough to provide the observed level of homogeneity and isotropy, we have  $\Delta\phi/m_{pl} \simeq (r/0.01)^{1/2}$ . Multiple field inflation models arising in string theory and other proposals for unification at high energies, as well as particle and string production during the inflationary period, can lead to even higher values of  $r$ .

Primordial gravitational waves imprint a unique, as yet undetected, signature in the CMB polarization. CMB polarization is a spin-two field on the sky, and is decomposed into the equivalent of a gradient—the E-mode—and a curl—the B-mode. Gravitational wave fluctuations are visible as the B-mode polarization of the CMB and are the only primordial contribution to B relevant at the time of recombination. Hence a detection of B-modes is a direct probe of  $r$ , and thus the energy scale of inflation and other primordial energetic processes. Furthermore, in the simple case of slow-roll inflation we have that  $r \approx -8n_T$ . Additional detailed measurements of the shape of the temperature and polarization spectra will measure higher derivatives of the inflationary potential.

The 2013 *Planck* data release has significantly improved previous constraints on inflationary models. In particular, and in the context of the simplest  $\Lambda$ CDM scenario, *Planck* results provide  $n_s = 0.9624 \pm 0.0075$  and  $r < 0.12$ . These results are notable because exact scale invariance (i.e.,  $n_s = 1$ ) of primordial perturbations is ruled out at more than  $5\sigma$ . When specific inflationary models are considered, *Planck* imposes significant constraints on the potential (Fig. 3), as discussed in Ref. [86]. Indeed *Planck* has shown that it is possible to test many inflation models using the CMB temperature data, yet even a forecast *Planck* limit  $r < 0.05$  would leave many interesting models unprobed. Given that the stochastic background of gravity waves is the smoking gun of inflation, it is crucial to map as accurately as possible the CMB polarization and in particular characterize the B-mode angular power spectrum.

To forecast how well we would be able to measure the power spectrum of the B-modes, it is important to recognize that the foreground signal is likely to dominate the cosmological signal at low  $\ell$ , where the most constraining information on  $r$  is situated. If we propagate the uncertainties connected to foreground contamination into the parameter error forecasts [107, 6, 9], we find that the proposed experimental set-up will enable us to explore most large field (single field) inflation models (i.e., where the field moves for  $\geq M_P$ ) and to rule in or out all large-field models, as illustrated in the right-hand panel of Fig. 3.

As the work by Smith et al. [98] indicates (see Fig. 8), the instrumental sensitivity, angular resolution and, as a result, foreground control and subtraction will enable us to achieve a detailed mapping of the lensing signal, and in particular to implement de-lensing techniques for the measurement of  $r$ , improving by a factor of three our constraint on  $r$ . This implies that *PRISM* will detect  $r \sim 3 \times 10^{-4}$  at more than  $3\sigma$ . This performance is very close, within factors  $\mathcal{O}(1)$ , to what an ideal experiment (i.e., with no noise and no foregrounds) could achieve, allowing *PRISM* to *directly* probe physics at an energy scale a staggering twelve orders of magnitude higher than the center-of-mass energy at the Large Hadron Collider (LHC).



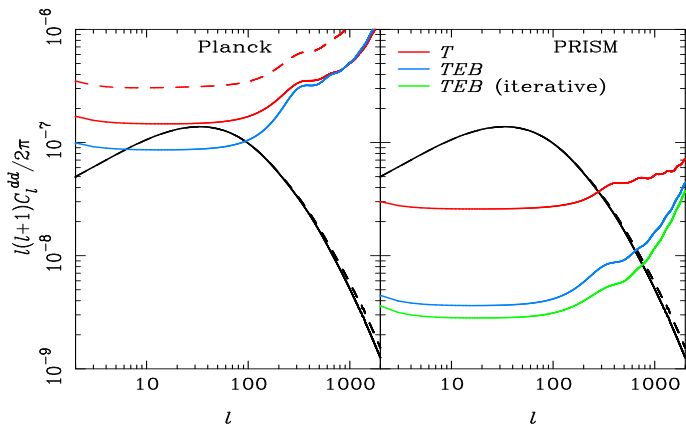


Figure 4: Reconstruction noise on the lensing deflection power spectrum forecast for the full *Planck* mission (four surveys; left) and *PRISM* (right) using temperature alone (red) and temperature and polarization (blue). For *Planck* we also show the approximate noise level for the temperature analysis of the nominal-mission data (red dashed) [81], and for *PRISM*, we also show the approximate noise level (green) for an improved iterative version of the reconstruction estimator. The deflection power spectrum is plotted based on the linear matter power spectrum (black solid) and with non-linear corrections (black dashed).

## 6 CMB at high resolution

The temperature anisotropies of the CMB have proved to be a remarkably clean probe of the high-redshift universe and have allowed the standard cosmological model to be tested to high precision. However, the accuracy of the recent results from *Planck*, based on the temperature anisotropies, are now close to being limited by errors in modelling extragalactic foregrounds. Fortunately, further progress can be made with the polarization anisotropies on small angular scales since the degree of polarization of the anisotropies is relatively larger there (around 4% by  $l = 2000$ ) than the foreground emission. By surveying the full polarized sky in many frequency bands, and with uniform calibration, *PRISM* will fully exploit the small-scale polarization of the CMB, improving significantly on results currently obtained from the temperature and those conceivably obtainable in the future with ground-based experiments.

**Probing the dark universe with CMB lensing:** Gravitational lensing of the CMB provides a clean probe of matter clustering integrated to high redshift. Lensing can be reconstructed from the CMB anisotropies via specific non-Gaussian signatures imprinted by the lenses. *Planck* has detected lensing via this route at the  $25\sigma$  level using the temperature anisotropies, but with low  $S/N$  per lensing mode. Polarization-based reconstructions from *PRISM* will be a major advance over *Planck*, achieving  $S/N \gg 1$  over individual multipoles up to  $l \approx 600$  over nearly the full sky (see Fig. 4). Significantly, *PRISM* can extract all of the information in the deflection power spectrum on scales where linear theory is reliable. To illustrate the power of the lensing measurements from *PRISM* in constraining physics that is inaccessible to the primary anisotropies alone due to degeneracies, we consider the mass of (light) neutrinos. Oscillation data constrain (squared) mass differences, and provide only lower bounds on the total mass summed over eigenstates: 0.06 eV and 0.1 eV for the normal and inverted hierarchy, respectively. These hierarchical limits provide natural targets for absolute mass measurements, but are well below the detection limits of current and future laboratory  $\beta$ -decay experiments. However, masses of these orders can be probed cosmologically via their effect on the clustering of matter. In  $w$ CDM models with massive neutrinos, we forecast a  $1\sigma$  error of 0.04 eV for the summed mass. This constraint can be improved further by combining with near-future BAO measurements, for example by a factor of almost two using BOSS, at which point it becomes possible to distinguish between the normal and inverted hierarchies (in the hierarchical limits) [43].

Lensing constraints from *PRISM* would be highly complementary to those from upcoming optical cosmic shear surveys, e.g., *Euclid*. The systematic effects are quite different with non-linearities being much less of an issue for CMB lensing and there are no intrinsic-alignment effects. The combination of the two probes of mass is particularly promising, since it allows calibration of multiplicative bias effects such as due to PSF corrections in the optical. Cross-correlating CMB lensing with other probes of large-scale structure, such as galaxies, the Ly $\alpha$  forest or CIB clustering (see Sec. 4), also has exceptional promise, allowing self-calibration of the tracer’s bias relation at the sub-percent level.

**Primordial non-Gaussianity:** Non-Gaussianity (NG) is now demonstrably a robust quantitative probe of cosmological physics [83]. *Planck* results dramatically improved previous NG analyses, offering the most stringent test to date of inflationary theory (with  $f_{\text{NL}}^{\text{loc}} = 2.7 \pm 5.8$ ) while also detecting for the first time ISW-lensing and diffuse point source bispectra. Already *Planck* offers enticing clues about the nontrivial ‘shape’ of the CMB bispectrum of our universe (see Fig. 5), the origin of which is yet to be explained. *PRISM* would offer the highest precision reconstructions of the CMB temperature and polarization bispectra and trispectra, which will provide a decisive and unambiguous probe of primordial cosmology back to the *Planck* era. At the same time, *PRISM* NG data will open new windows for investigating dark energy and gravitational physics,

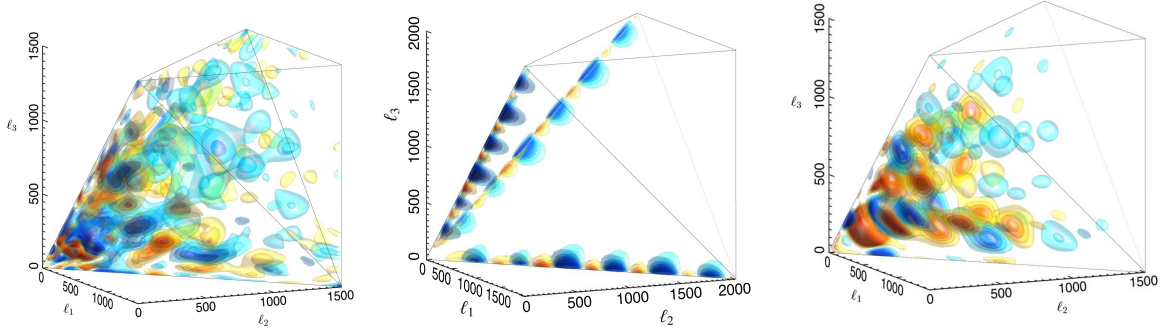


Figure 5: *Planck* CMB temperature bispectrum [83] (left) and primordial (right) and late-time (middle) non-Gaussian shapes [83, 82]. Note the periodic CMB ISW-lensing signal (middle) in the squeezed limit along the edges, which is seen at the  $2.5\sigma$  level in the *Planck* bispectrum on the left. Scale-invariant signals predicted by many inflationary models are strongly constrained by the *Planck* bispectrum, although ‘oscillatory’ and ‘flattened’ features hint at new physics. An example of an inflationary ‘feature’ model is shown on the right. *PRISM* will probe these hints with an order of magnitude more resolved triangle configurations.

as well as astrophysical sources, large-scale structure and galactic history.

A unique advantage of the CMB for probing NG is its ability to recognize the distinct patterns that physical mechanisms leave in the *shape* of higher-order correlators (Fig. 5). *PRISM* will allow a vastly enhanced exploration of physically-predicted NG shapes compared to any other projected probe of NG. For example, the constraint volume in bispectrum space spanned by the local, equilateral and flattened bispectra will reduce by a factor of 75 compared to the current *Planck* volume, and a factor of 30 over that predicted from the full-mission *Planck* data (including polarization). From polarization maps alone (which provide information independent of the temperature maps), we expect a volume reduction factor from the full-mission *Planck* data to *PRISM* of order 110. Moreover, local-model trispectrum parameters could be measured with a precision  $\Delta g_{\text{NL}} = 3 \times 10^4$  and  $\Delta \tau_{\text{NL}} = 1 \times 10^2$  [97]. These could investigate consistency conditions between polyspectra, which can be used to test large classes of multi-field inflation models in addition to single-field inflation. There are other alternative inflationary scenarios for which an observable non-Gaussian signal is quite natural, e.g., those with features or periodicity in the inflationary potential (Fig. 5). Each of these models has a distinct fingerprint, many uncorrelated with the standard three primordial shapes and, in all cases, *PRISM* would significantly improve over present *Planck* constraints, offering genuine discovery potential. Beyond searches for primordial NG, *PRISM* is guaranteed to make important observations of late-time NG. For example, it will decisively detect and characterize the lensing-ISW correlation, driven by dark energy, achieving a  $9\sigma$  detection, resulting in a new probe of dark energy physics from the CMB alone.

**Parameters from high-resolution polarization spectra:** *PRISM* will measure the CMB angular power spectra with outstanding precision to small angular scales. In particular, in the 105–200 GHz frequency range, the relatively clean *EE* polarization spectrum is cosmic-variance limited to  $l = 2500$  (and the *BB* spectrum from lensing to  $l = 1100$ ). Such a remarkable measurement of the polarization of the CMB damping tail will be an invaluable source of information on the shape of the primordial power spectrum and the fundamental matter content of the Universe. For example, in  $\Lambda$ CDM models, the spectral index and its running will be measured more precisely than with current *Planck* data by factors of five and three, respectively. The Hubble constant (a point of tension between *Planck* data and direct astrophysical measurements) will be measured a factor of 10 better than currently (and 2.5 times better than expected from the full *Planck* data). Fundamental questions about the matter content include the effective number of relativistic species  $N_{\text{eff}}$ , for which a non-standard value (which can relieve the *Planck*– $H_0$  tension) could be due to sterile neutrinos, as advocated in particle physics to explain certain anomalies in the neutrino sector, the helium abundance  $Y_{\text{P}}$ , which provides a clean test of standard BBN, the neutrino mass, and the dark matter annihilation cross-section. In one-parameter extensions of  $\Lambda$ CDM, *PRISM* will measure  $N_{\text{eff}}$  to 2% precision and  $Y_{\text{P}}$  to 1%. These values indicate that a  $2\sigma$  anomaly hinted at by *Planck* could be confirmed decisively with *PRISM*. Moreover, from its measurement of the *B*-mode power spectrum, *PRISM* should extend the range of sensitivity to cosmic strings by an order of magnitude over the recent *Planck* constraints [82, 1].

## 7 CMB spectral distortions

*COBE/FIRAS* has shown that the average CMB spectrum is extremely close to a perfect blackbody, with

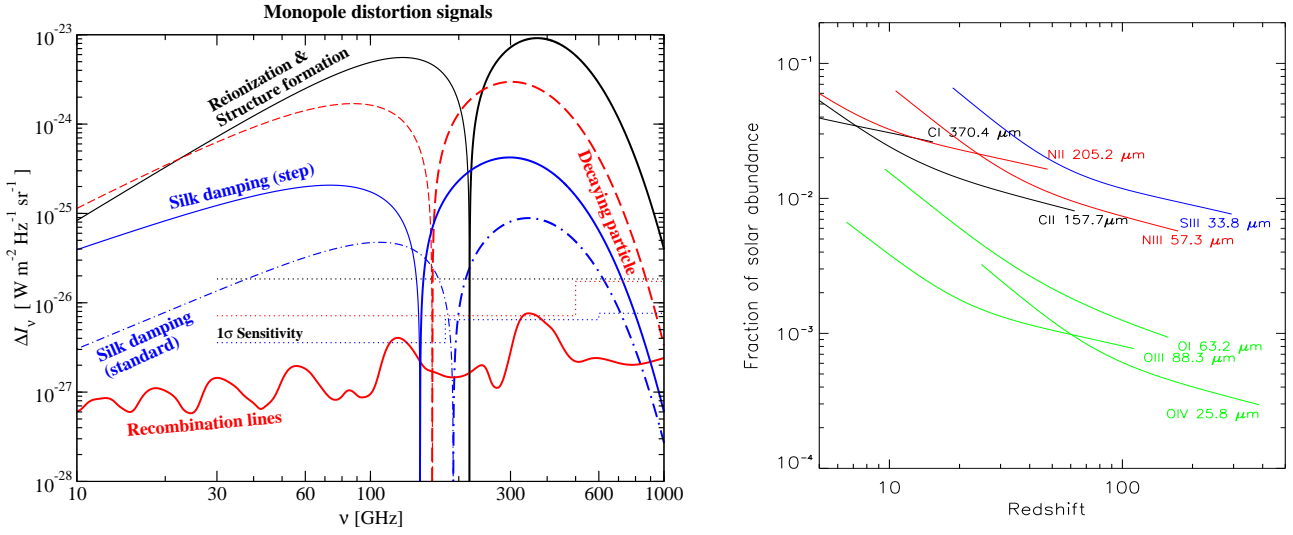


Figure 6: Left: spectral distortions for different scenarios. Thick lines denote positive, and thinner lines negative signal. The  $1\sigma$  sensitivities of *PRISM* for different designs are also indicated. Right: projected constraints on different metal ions.

possible departures limited to  $\Delta I_\nu/I_\nu \lesssim (\text{few}) \times 10^{-5}$  [68, 37]. This places very tight constraints on the thermal history of our Universe, ruling out cosmologies with extended periods of significant energy release at redshifts  $z \lesssim (\text{few}) \times 10^6$  [108, 100, 54, 30, 12, 49, 16, 22, 58]. There are, however, a large number of astrophysical and cosmological processes that cause (inevitable) spectral distortions of the CMB at a level that has only come within reach of present-day technology. With *PRISM* an unexplored window to the early universe will be opened, allowing detailed studies of (see Fig. 6 for illustration):

**Reionization and structure formation:** Radiation from the first stars and galaxies [53, 2], feedback by supernovae [73] and structure formation shocks [101, 14, 71] heat the IGM at redshifts  $z \lesssim 10 - 20$ , producing hot electrons that up-scatter CMB photons, giving rise to a Compton  $y$ -distortion with average amplitude  $\Delta I_\nu/I_\nu \simeq 10^{-7} - 10^{-6}$ . This signal will be detected at more than a  $100\sigma$  by *PRISM*, providing a sensitive probe of reionization physics and delivering a census of the missing baryons in the local Universe. *PRISM* furthermore has the potential to separate the spatially varying signature caused by the WHIM and proto-clusters [109]. It also offers a unique opportunity to observe the free-free distortion associated with reionization, providing a complementary way to study the late evolution of inhomogeneities [87].

**Decaying and annihilating relics:** The CMB spectrum will establish tight limits on decaying and annihilating particles in the pre-recombination epoch [50, 29, 69, 17, 22]. This is especially interesting for decaying particles with lifetimes  $t_X \simeq 10^8 - 10^{10}$  sec, as the exact shape of the distortion encodes when the decay occurred [22, 59, 18, 19]. *PRISM* therefore provides an unprecedented probe of early-universe particle physics, with many natural particle candidates found in supersymmetric models [36, 35].

**Constraining inflation:** Silk damping of small-scale perturbations gives rise to CMB distortions [100, 28, 3, 52] which directly depend on the shape and amplitude of the primordial power spectrum at scales  $0.6 \text{ kpc} \lesssim \lambda \lesssim 1 \text{ Mpc}$  (or multipoles  $10^5 \lesssim \ell \lesssim 10^8$ ) [25, 62]. This allows constraining the trajectory of the inflaton at stages unexplored by ongoing or planned experiments [24, 88, 60], extending our reach from 7  $e$ -folds of inflation probed with the CMB anisotropies to a total of 17  $e$ -folds. The signal is also sensitive to the difference between adiabatic and isocurvature perturbations [3, 51, 31, 20], as well as primordial non-Gaussianity in the ultra squeezed-limit, leading to a spatially varying spectral signal that correlates with CMB temperature anisotropies as large angular scales [75, 38]. A competing monopole signal, characterized by a *negative*  $\mu$ - and  $y$ -parameter, is introduced by the adiabatic cooling of ordinary matter [16, 22, 61], to which *PRISM* will also be sensitive.

**Metals during the dark ages:** Any scattering of CMB photons after recombination blurs CMB anisotropies at small scales, while producing new anisotropies at large scales. Electrons from the reionization epoch are the dominant source of optical depth, causing a signature already detected by WMAP and Planck [7, 84]. The resonant scattering of CMB photon by fine structure lines of metals and heavy ions produced by the first stars adds to this optical depth, making it frequency-dependent [5]. By comparing CMB temperature and polarization anisotropies at different frequencies one can thus determine the abundances of ions such as OI, OIII, NII, NIII, CI, CII at different redshifts [46, 48]. Furthermore, UV radiation emitted by the first

stars can push the OI  $63.2\ \mu\text{m}$  and CII  $157.7\ \mu\text{m}$  transitions out of equilibrium with the CMB, producing a distortion  $\Delta I_\nu/I_\nu \simeq 10^{-8} - 10^{-9}$  due to fine structure emission [41, 47], providing yet another window to reionization within reach of *PRISM*.

**Cosmological recombination radiation:** The recombination of H and He [34] at redshifts  $z \simeq 10^3 - 10^4$ , corresponding to  $\simeq 260\ \text{kyr}$  (HI),  $\simeq 130\ \text{kyr}$  (HE I), and  $\simeq 18\ \text{kyr}$  (HE II) after the big bang [93, 21, 94]. The signal provides an independent determination of the cosmological parameters (such as the baryon density and *pre-stellar* helium abundance) and direct measurements of the recombination dynamics, probing the Universe at stages well before the last scattering surface [99]. The effect on the TT power spectrum introduced by resonance scattering of CMB photons by the first lines of the Balmer and Paschen series [92, 45, 48] will also be detectable with *PRISM*, providing an additional opportunity to directly constrain the recombination history and obtain independent determinations of cosmological parameters (e.g.  $\Omega_b$  or  $\Omega_m$ ).

**Non-Gaussianity:** CMB spectral distortions can also provide a new probe of primordial NG [76]. We know almost nothing about NG on the small scales that can be probed via these observations. In particular, the cross-correlation between  $\mu$ -type distortions and CMB anisotropies is naturally sensitive to the very squeezed limit of the primordial bispectrum (probing scales as small as  $50 \leq k\ \text{Mpc} \leq 10^4$ ). Also, the power spectrum of  $\mu$ -distortions can probe the trispectrum of primordial fluctuations. Such measurements can be particularly constraining for models where the primordial power spectrum grows on small scales (see e.g. [23]), and values  $f_{\text{NL}}^{\text{loc}} < 1$  can be achieved. Also,  $\mu$ -type distortions can shed light on non-standard initial states for the quantum fluctuations. For a large class of inflationary models characterized by a non-Bunch-Davies vacuum (whose bispectrum is enhanced in the squeezed limit with respect to the local form) a high  $S/N$  can be achieved [39].

All these examples demonstrate that the CMB spectrum provides a rich and unique source of complementary information about the early Universe, with the certainty of a detection of spectral distortions at a level within reach of *PRISM*'s capabilities. The CMB spectrum will also establish interesting constraints on the power spectrum of small-scale magnetic fields [57], cosmic strings [74, 103, 104], evaporating primordial black holes [13], decay of vacuum energy density [4, 11, 29], and other new physics [67, 10], to mention a few more exotic examples. Deciphering all these signals will be a big challenge for the future. This area has great potential for new discoveries and for providing new independent constraints on unexplored processes that cannot be explored by other means.

## 8 Structure of the dusty magnetized Galactic ISM

The data analysis is still on-going but it is already clear that *Herschel* and *Planck* will have a profound and lasting impact on our understanding of the interstellar medium and star formation. *PRISM* holds even greater promise for breakthroughs. Dust and synchrotron radiation are the dominant contributions to the sky emission and polarization to be observed by *PRISM*. Dust emission is an optically thin tracer of the structure of interstellar matter. Synchrotron radiation traces the magnetic field over the whole volume of the Galaxy, while dust polarization traces the magnetic field within the thin star forming disk, where the interstellar matter is concentrated. *PRISM* will image these two complementary tracers with unprecedented sensitivity and angular resolution. It will also provide all-sky images of spectral lines, which are key diagnostics of interstellar gas physics. No other initiative offers a comparable imaging capability of interstellar components over as wide a range of scales. In the following subsections we detail how *PRISM* will address three fundamental questions of Galactic astrophysics: (1) What are the processes that structure the interstellar medium? (2) What role does the magnetic field play in star formation? (3) What are the processes that determine the composition and evolution of interstellar dust?

### 8.1 Structure of interstellar medium

*Herschel* far infrared observations have provided astronomers new insight into how turbulence stirs up the interstellar gas, giving rise to a filamentary, web-like structure within the diffuse interstellar medium and molecular clouds. *PRISM* will extend the *Herschel* dust observations to the whole sky and provide unique data on emission lines key to quantifying physical processes. The spectral range of *PRISM* includes atomic and molecular lines that serve as diagnostics of the gas density and temperature, its chemical state, and energy budget. *Herschel* has observed these lines along discrete lines of sight with very limited imaging. By

mapping these lines and dust emission over the whole sky at an angular resolution comparable to that of *Herschel*, *PRISM* will probe the connection between the structure of matter and gas cooling across scales.

The *PRISM* sky maps will provide multiple clues to characterize the physical processes that shape interstellar matter. The CII, CI, and OI fine structure lines and the rotational lines of CO and H<sub>2</sub>O are the main cooling lines of cold neutral medium and molecular clouds and probe local physical conditions and the exchange of energy associated with the formation of molecular gas within the diffuse interstellar medium and of stars within molecular clouds. The NII lines at 122 and 205  $\mu\text{m}$  are spectroscopic tracers of the ionized gas. These lines are essential for distinguishing the contribution of neutral and ionized gas to the CII emission. *PRISM* will have the sensitivity to image the CII line emission at sub-arcminute resolution even at the Galactic poles. The CII map can be combined with HI and dust observations to study the formation of cold gas from the warm neutral medium through the thermal instability. This analysis will probe the expected link, yet to be confirmed observationally, between the small-scale structure of the cold interstellar medium and gas cooling. The CII line emission is also key to studying the formation of molecular gas by tracing the CO-dark H<sub>2</sub> gas [78]. In star forming molecular clouds, the CO, CI, OI, and H<sub>2</sub>O lines are the key tracers of the processes creating the initial conditions of star formation and of the feedback from newly formed stars on their parent clouds.

## 8.2 Galactic magnetic field and star formation

Star formation results from the action of gravity, counteracted by thermal, magnetic, and turbulent pressures [44]. For stars to form, gravity must locally become the dominant force. This happens when the turbulent energy has dissipated and matter has condensed without increasing the magnetic field by a comparable amount. What are the processes that drive and regulate the rate at which matter reaches this stage? This is a long standing question to which theorists have over the decades offered multiple explanations, focusing on either ambipolar diffusion, turbulence, or magnetic reconnection to decouple matter from the magnetic field and allow the formation of condensations of gas in which stars may form [27].

*PRISM* observations of the polarization in the far-IR and sub-mm will provide unique clues to understand the role of the magnetic field in star formation. Compared to synchrotron radiation and Faraday rotation, dust polarization images the structure of the magnetic field through an emission process tracing matter. It is best suited to characterize the interplay between turbulence, gravity, and the Galactic magnetic field. The *PRISM* data will provide unique data to study magneto-hydrodynamical turbulence because it will drastically increase the spectral range of accurately probed magneto-hydrodynamical modes. The data will provide unprecedented statistical information to characterize the energy injection and energy transfer down to the dissipation scales.

Polarization data from the *PRISM* survey will have the sensitivity and angular resolution required to map continuously the Galactic magnetic field over the whole sky down to sub-arcminute resolution even at the Galactic poles. The wide frequency range of the mission will measure polarization for separate emission components with distinct temperatures along the line of sight. *PRISM* will provide a new perspective on the structure of the magnetic field in molecular clouds, independent of grain alignment, by imaging the polarization of CO emission in multiple rotational lines [40]. No project offers comparable capabilities. Planck has provided the first all-sky maps of dust polarization with 5' resolution but the data is sensitivity limited even at the highest Planck frequency (353 GHz). Ground based telescopes at sub-mm and millimeter wavelengths of bright compact sources at arcsecond resolution (for example with ALMA) complement the full-sky survey of extended emission from the diffuse interstellar medium and molecular clouds that only *PRISM* can carry out.

## 8.3 Nature of interstellar dust

The combination of spectral and spatial information provided by *PRISM* will provide new tools for studying the interstellar dust, in particular its nature and its evolution. Dust properties (e.g., size, temperature, emissivity) are found to vary from one line of sight to another within the diffuse interstellar medium and molecular clouds. These observations indicate that dust grains evolve in a manner depending on their environment within the interstellar medium. They can grow through the formation of refractory or ice mantles, or by coagulation into aggregates in dense and quiescent regions. They can also be destroyed by fragmentation and erosion of their mantles under more violent conditions. The composition of interstellar dust reflects the action of interstellar processes, which contribute to breaking and reconstituting grains over timescales

much shorter than the timescale of injection by stellar ejecta. While there is broad consensus on this view of interstellar dust, the processes that drive its evolution in space are poorly understood [32]. Understanding interstellar dust evolution is a major challenge in astrophysics underlying key physical and chemical processes in interstellar space. In particular, to fully exploit the *PRISM* data we will need to characterize where in the interstellar medium grains are aligned with respect to the Galactic magnetic field and with what efficiency.

Large dust grains (size  $> 10$  nm) dominate the dust mass. Within the diffuse interstellar medium, these grains are cold ( $\sim 10 - 20$  K) and emit within the *PRISM* frequency range. Dipole emission from small rapidly spinning dust particles constitutes an additional emission component, known as anomalous microwave emission. Magnetic dipole radiation from thermal fluctuations in magnetic nano-particles may also be a significant emission component over the frequency range relevant to CMB studies [33]. To achieve the *PRISM* objectives on CMB polarization, it is necessary to characterize the spectral dependence of the polarized signal from each of these dust components with high accuracy across the sky. This is a challenge but also a unique opportunity for dust studies. The spectral energy distribution of dust emission and the polarization signal can be cross-correlated with the spectral diagnostics of the interstellar medium structure to characterize the physical processes that determine the composition and evolution of interstellar dust. The same data analysis will also elucidate the physics of grain alignment.

*PRISM* will also probe the zodiacal dust emission from within our solar system. The fact that *PRISM* scans a substantial portion of the sky each day allows for a three-dimensional tomographic mapping of the zodiacal emission. Understanding zodiacal emission is crucial both to understanding our solar system and to carrying out a complete foreground separation.

## 9 Strawman mission concept

The science program above requires measuring the sky brightness and polarization at high angular resolution and in many frequency bands across a wide spectral range. It also requires measuring the absolute spectrum of the sky background with moderate angular and spectral resolution. As a baseline, we propose to perform the best possible spectro-polarimetric sky survey in the 30-6000 GHz frequency range with two instruments optimized for best joint performance sharing a single platform in orbit around the Sun-Earth L2 Lagrange point: (1) a *polarimetric imager* (PIM) observing with about 30 broad and 300 narrow spectral bands with a diffraction limited angular resolution and a sensitivity limited by the photon noise of the sky emission itself; and (2) an *absolute spectro-photometer* (ASP) that will measure sky emission spectra with a spectral resolution between 500 MHz and 15 GHz and an angular resolution of about  $1.4^\circ$ . These complementary instruments will map simultaneously the absolute sky intensity and polarization with high sensitivity and with high spectral or spatial resolution. The data from both instruments can be binned (in frequency) and smoothed to obtain matching observations with  $\delta\nu/\nu \approx 0.25$  and  $1.4^\circ$  resolution, allowing on-sky inter-calibration on large scales (and hence absolute calibration of the PIM). This will also enable correction of the ASP spectra from foreground contamination using high resolution component maps extracted from PIM data (e.g., large clusters  $y$ -distortion in the ASP data and line emission from emitting regions unresolved in the coarse resolution ASP maps).

As the scientific outcome of this mission depends on the complementarity of both instruments and on the control of systematic errors, a careful optimization of the ASP and the PIM (number and bandwidth of spectral bands vs. sensitivity) and of the mission (scanning strategy, joint analysis tools) with comprehensive simulations is an essential future phase of the mission study.

The focal planes of both instruments will be cooled to 0.1K using a cryogenic system adapted from that of *Planck*, with continuous recycling of the gases for an improved mission duration of 4 years (baseline) or longer.

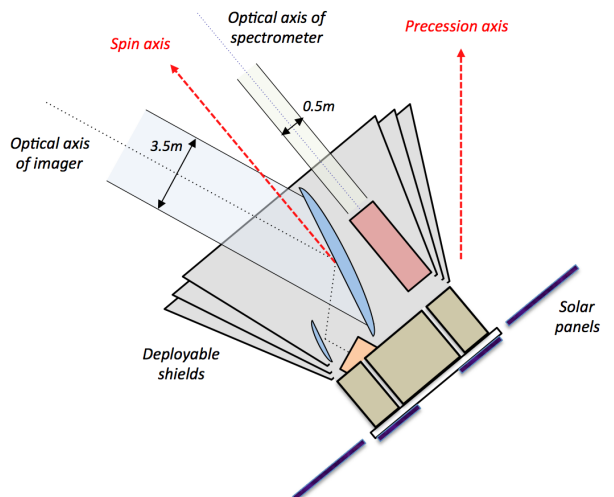


Figure 7: The *PRISM* spacecraft with its two instruments: PIM, with a 3.5-diameter telescope with a FOV at  $\sim 30^\circ$  from the spacecraft spin axis, and ASP, aligned with the spin axis.

## 9.1 Instruments

$\nu_0$ GHz	Range GHz	$\Delta\nu/\nu$	$n_{det}$	$\theta_{fwhm}$	$\sigma_I$ per det 1 arcmin		$\sigma_{(Q,U)}$ per det 1 arcmin		Main molec. & atomic lines
					$\mu K_{RJ}$	$\mu K_{CMB}$	$\mu K_{RJ}$	$\mu K_{CMB}$	
30	26-34	.25	50	17'	61.9	63.4	87.6	89.7	
36	31-41	.25	100	14'	57.8	59.7	81.7	84.5	
43	38-48	.25	100	12'	53.9	56.5	76.2	79.9	
51	45-59	.25	150	10'	50.2	53.7	71.0	75.9	
62	54-70	.25	150	8.2'	46.1	50.8	65.2	71.9	
75	65-85	.25	150	6.8'	42.0	48.5	59.4	68.6	
90	78-100	.25	200	5.7'	38.0	46.7	53.8	66.0	HCN & HCO <sup>+</sup> at 89 GHz
105	95-120	.25	250	4.8'	34.5	45.6	48.8	64.4	CO at 110-115 GHz
135	120-150	.25	300	3.8'	28.6	44.9	40.4	63.4	
160	135-175	.25	350	3.2'	24.4	45.5	34.5	64.3	
185	165-210	.25	350	2.8'	20.8	47.1	29.4	66.6	HCN & HCO <sup>+</sup> at 177 GHz
200	180-220	.20	350	2.5'	18.9	48.5	26.7	68.6	
220	195-250	.25	350	2.3'	16.5	50.9	23.4	71.9	CO at 220-230 GHz
265	235-300	.25	350	1.9'	12.2	58.5	17.3	82.8	HCN & HCO <sup>+</sup> at 266 GHz
300	270-330	.20	350	1.7'	9.6	67.1	13.6	94.9	
320	280-360	.25	350	1.6'	8.4	73.2	11.8	103	CO, HCN & HCO <sup>+</sup>
395	360-435	.20	350	1.3'	4.9	107	7.0	151	
460	405-520	.25	350	1.1'	3.1	156	4.4	221	CO, HCN & HCO <sup>+</sup>
555	485-625	.25	300	55''	1.6	297	2.3	420	C-I, HCN, HCO <sup>+</sup> , H <sub>2</sub> O, CO
660	580-750	.25	300	46''	0.85	700	1.2	990	CO, HCN & HCO <sup>+</sup>
					nK <sub>RJ</sub>	kJy/sr	nK <sub>RJ</sub>	kJy/sr	
800	700-900	.25	200	38''	483	9.5	683	13.4	
960	840-1080	.25	200	32''	390	11.0	552	15.6	
1150	1000-1300	.25	200	27''	361	14.6	510	20.7	
1380	1200-1550	.25	200	22''	331	19.4	468	27.4	N-II at 1461 GHz
1660	1470-1860	.25	200	18''	290	24.5	410	34.7	
1990	1740-2240	.25	200	15''	241	29.3	341	41.5	C-II at 1900 GHz
2400	2100-2700	.25	200	13''	188	33.3	266	47.1	N-II at 2460 GHz
2850	2500-3200	.25	200	11''	146	36.4	206	51.4	
3450	3000-3900	.25	200	8.8''	113	41.4	160	58.5	O-III at 3393 GHz
4100	3600-4600	.25	200	7.4''	98	50.8	139	71.8	
5000	4350-5550	.25	200	6.1''	91	70.1	129	99.1	O-I at 4765 GHz
6000	5200-6800	.25	200	5.1''	87	96.7	124	136	O-III at 5786 GHz

Table 1: The 32 broad-band channels of the polarized imager with a total of 7600 detectors. Sensitivities are averages for sky regions at galactic latitude and ecliptic latitude both higher than 30°. A detector noise level equal to the sky photon noise is assumed. The mission sensitivity per frequency channel is the sensitivity per detector divided by  $\sqrt{n_{det}}$ .

**The polarimetric imager:** The optical configuration relies on a dual off-axis mirror telescope with a 3.5 m projected aperture diameter primary and a 0.8 m diameter secondary coupled to a multi spectral band polarimeter. The broad-band PIM comprises 32 main channels of  $\delta\nu/\nu \approx .25$  relying on dual-polarized pixel arrays (Table 1). At frequencies below 700 GHz, the emphasis is on the sensitivity and control of systematics for CMB and SZ science.

The whole frequency range will also be covered at higher spectral resolution ( $\delta\nu/\nu \approx .025$ ) to map spectral lines. The  $\sim 300$  frequency channels (not listed in Table 1) will be obtained using antenna coupled bolometers and channelizers to split the spectral band of each broad-band horn into 5-10 narrow frequency bands, with similar numbers of narrow-band and broad-band detectors. The sensitivity to continuum emission per detector is reduced in the narrow-band channels as compared to the broad-band channels, but the sensitivity to spectral lines is better by a factor of about 2-3.

**The absolute spectrophotometer:** A Martin-Puplett Fourier Transform Spectrometer (FTS) will allow for a large throughput and sensitivity, differential measurements (the sky is compared to an internal blackbody calibrator as in COBE-FIRAS), and a variable spectral resolution. Dichroics at the two output ports can optionally split the full 30 - 6000 GHz range into sub-bands with reduced photon noise. The instrument is cooled at 2.7K, so that the bolometric detector sensitivity is limited by photon noise from the sky. Two operating modes are available: high-resolution ( $\Delta\nu \sim 0.5$  GHz) and low-resolution ( $\Delta\nu \sim 15$  GHz). The sensitivity of the high-resolution mode is 30 times worse than for the low-resolution mode. The instrument beam is aligned with the spin axis of the satellite, so that precession has a negligible effect during the

interferogram scan ( $\sim 1\text{s}/10\text{s}$  long in the low-res/high-res mode). The main characteristics for three possible configurations of the instrument are detailed in Table 2.

Band (GHz)	Resolution (GHz)	$A\Omega$ ( $\text{cm}^2\text{sr}$ )	Background (pW)	NEP $\nu$ ( $\text{W}/\text{m}^2/\text{sr}/\text{Hz}\times\sqrt{\text{s}}$ )	Global 4-yr mission sensitivity ( $\text{W}/\text{m}^2/\text{sr}/\text{Hz}$ )
30-6000	15	1	150	$1.8 \times 10^{-22}$	$1.8 \times 10^{-26}$
30-500	15	1	97	$7.0 \times 10^{-23}$	$7.2 \times 10^{-27}$
500 - 6000	15	1	70	$1.7 \times 10^{-22}$	$1.7 \times 10^{-26}$
30-180	15	1	42	$3.5 \times 10^{-23}$	$3.6 \times 10^{-27}$
180-600	15	1	57	$6.3 \times 10^{-23}$	$6.5 \times 10^{-27}$
600-3000	15	1	20	$7.4 \times 10^{-23}$	$7.6 \times 10^{-27}$
3000-6000	15	1	28	$1.6 \times 10^{-22}$	$1.6 \times 10^{-26}$

Table 2: FTS performance of three possible configurations for photon noise limited detectors. With an entrance pupil 50 cm in diameter, the baseline throughput is  $\sim 1 \text{ cm}^2\text{sr}$  and the angular resolution  $1.4^\circ$ . The theoretical monopole sensitivity for each spectral bin is reported in the last column assuming 4 years of observation and 75% useful sky. The actual sensitivity, taking into account efficiency factors can be 2-3 times worse. Line 1 is a configuration with an ultra-wide spectral coverage obtained with one detector in both output ports. In lines 2-3 the detectors at the output ports are sensitive to different bands. In lines 4-7 each output port is split into two sub-bands using dichroics to minimize photon noise in the low-frequency bins.

Using detectors with  $A\Omega \sim 1 \text{ cm}^2\text{sr}$  and angular resolution  $\sim 1.4^\circ$ , we estimate that the CIB can be measured with  $S/N = 10$  in a fraction of a second at 1500 GHz and in  $\sim 10$  seconds at 140 GHz, while a  $y$ -distortion  $\sim 10^{-8}$  can be measured with  $S/N = 10$  at 350 GHz in two hours of integration. Recombination lines could be measured integrating over the whole mission if the overall stability of the instrument and the quality of the reference blackbody are sufficient.

The main issue for this instrument is the control of systematic effects. The instrument design allows for a number of zero tests and cross-checks on the data. The main problem is to control the blackness of the reference and calibration blackbodies with the required accuracy. Reflectivities lower than  $R = -50/-60$  dB have been obtained in the frequency range of interest in the Planck and ARCADE references. We plan to achieve  $R < -70$  dB building on these experiences through a combination of electromagnetic simulations and laboratory emissivity measurements on improved shapes and space-qualified materials.

## 9.2 Scan strategy

The observing strategy must provide: (1) full sky coverage for both instruments; (2) cross-linked scan paths and observation of all sky pixels in many orientations for all detectors of the PIM; (3) fast scanning of the PIM to avoid low-frequency drifts; (4) slow scanning for the ASP field of view to allow for few seconds long interferogram scans with negligible depointing; (5) avoiding direct solar radiation on the payload. These requirements can be satisfied by a spinning spacecraft with the ASP aligned along the spin axis and the PIM offset by  $\theta_{\text{spin}} \approx 30^\circ$  (Fig. 7). During each spacecraft rotation (with  $\omega_{\text{spin}}$  of a few rpm), the PIM scans circles of diameter  $\approx 2\theta_{\text{spin}}$  while the APS rotates in place. A slow precession of the spin axis (with a period between a few hours and one day) with a precession angle  $\theta_{\text{prec}} \approx 45^\circ$  results in slow scans of the ASP on large circles of diameter  $2\theta_{\text{prec}}$ . Finally, the precession axis evolves by about  $1^\circ$  per day along the ecliptic plane to keep the payload away from the Sun, and also slowly moves perpendicular to the ecliptic plane so as to map the ecliptic poles. Deployable screens isolate the payload from the heat from the Sun, providing a first stage of passive cooling to  $\approx 40$  K.

## 9.3 Experimental challenges

**Telescope temperature:** Actively cooling the telescope to 4 K (mission objective) instead of 40 K (achievable by passive cooling) substantially improves the sensitivity, especially for frequencies above 200 GHz. *PRISM* will benefit from the development activities for the SPICA mission, the telescope of which is based on a 3.5 m diameter primary cooled to 5 K.

**Polarization modulation:** The baseline, similar to the solution proposed in the previous SAMPAN and EPIC studies, relies on the scanning strategy and the rotation of the entire payload. However alternative strategies such as the use of a half-wave plate in front of the focal plane (the receivers being the major source of instrumental polarization) could be considered during a trade-off analysis.



$\nu_c$ ange	Req. NEP	Req. $\tau$	Focal plane technology			
			Detector technology		Optical coupling	
			Baseline	Backup	Baseline	Backup
30-75	3.3 – 5.7	2.96 – 1.18	TES	HEMT	MPA/CSA	HA
90-320	4.6 – 7	1.18 – 0.4	TES	KIDS	HA+POMT	MPA
395-660	0.94 – 3.1	0.4 – 0.13	TES	KIDS	MPA/CSA	LHA
800-6000	0.011 – 0.63	0.13 – 0.01	KIDS	HEB/CEB	MPA/CSA	LHA

Table 3: Required NEP and time constants for various frequency ranges and corresponding baseline and backup focal plane technology. TES: Transition Edge Sensors (Technology Readiness Level 5); HEMT: High Electron Mobility Transistor (TRL 5); KID: Kinetic Inductance Detector (TRL 5); HEB: Hot Electron Bolometer (TRL 4); CEB: Cold Electron Bolometer (TRL 3); HA: Horn Array (TRL 9); LHA: Lithographed Horn Array (TRL 5); MPA: Multichroic Planar Antenna (TRL 4); CSA: Crossed Slot Antenna (TRL 5); POMT: Planar Ortho-Mode Transducer (TRL 5)

**Detectors:** Direct detectors (such as TES bolometers, CEBs or KIDs) are the most sensitive detectors at mm wavelengths. Bolometers have achieved photon noise limited in-flight performance with the Planck [105] and Herschel [42] missions. Large bolometer arrays with thousands of pixels are currently used on large ground-based telescopes. They are currently not proven as a viable technology for 30 to 70 GHz but it is likely that their efficiency will improve in the next few years at low frequencies. For instance studies [64] have shown that 70 GHz CEBs could lead to NEPs of  $(\text{few}) \times 10^{-18} W \cdot Hz^{1/2}$ . As an alternative solution, the *PRISM* instruments could take advantage of the recent breakthroughs in cryogenic HEMT technology, with sensitivities predicted to reach 2-3 times the quantum limit up to 150-200 GHz (instead of 4-5 times up to 100 GHz so far). In addition, these devices allowing for cryogenically cooled miniaturized polarimeter designs will simplify the thermo-mechanical design. Hence, while a single detector technology throughout the instruments would be preferable, the option of using a combination of HEMTs and bolometers remains open (Table 3).

**Detector time constants:** The fast scanning of the *PRISM* mission requires fast detector time constants, of order 1 ms at 100 GHz, down to  $\sim 10 \mu s$  at 6 THz. These time constants are challenging (especially at high frequencies), but have already been achieved with recent TESs, KIDs or CEBs.

## 9.4 Ancillary spacecraft

We propose that the mission include a small ancillary spacecraft serving the following functions:

**Telecommunication:** The high resolution mapping of the full sky with the many detectors of *PRISM* with a lossless compression of 4 gives a total data rate of  $\sim 350$  Mbit/s (of which 300 Mbit/s is from the channels above 700 GHz). Further on-board reduction by a factor  $\sim 10-20$  can be achieved by averaging the timelines of detectors following each other on the same scan path (after automatic removal of spikes due to cosmic rays) to yield a total data rate  $< 40$  Mbit/s (a few times greater than Euclid or Gaia). A phased-array antenna or counter-rotating antenna on the main spacecraft is an option. Decoupling the communication function from the main spacecraft using an ancillary spacecraft as an intermediate station for data transmission will allow for a maximally flexible scanning strategy for the best polarization modulation and full sky coverage.

**In-flight calibration:** The hardest *PRISM* design problem is ensuring that the performance is limited by detector noise rather than systematic effects and calibration uncertainties. While pre-flight calibration is necessary, an ancillary spacecraft fitted with calibrated, polarized sources could be used for precise in-flight calibration of the polarization response and polarization angles of the detectors, and for main beams and far sidelobe measurements down to extremely low levels (below -140 dB) at several times during the mission lifetime.

## 10 Competition and complementarity with other observations

**B-mode experiments:** Searching for primordial gravitational waves through B-mode polarization is the principal science driver of numerous suborbital experiments (e.g., *BICEP*, *QUIET*, *SPIDER*, *ACTPol*, *SPT-Pol*, *QUBIC*, *EBEX*, *PolarBear*, *QUIJOTE*) despite considerable limitations due to atmospheric opacity, far-side lobe pickup from the ground, and unstable observing conditions that make controlling systemic errors especially difficult, particularly on the largest angular scales where the B mode signal is largest. Forecasts of  $r$  from ground-based experiments are often impressive but assume very simple foregrounds. For this reason a detection of  $r$  from the ground would provide a strong motivation for a confirmation and more precise

characterization from space. Moreover, two US space missions concepts, *CMBPol* and *PIXIE*, and one in Japan, *LiteBird*, have been proposed, but none has yet been funded. Among the current space mission concepts, *PRISM* is the most ambitious and encompasses the broadest science case. *LiteBird* is a highly-targeted, low-cost Japanese B-mode mission concept, in many respects similar to the *BPol* mission proposed to ESA in 2007. With its coarse angular resolution and limited sensitivity, *LiteBird* would be able to detect B-modes assuming that  $r$  is not too small and that the foregrounds are not too complicated. *LiteBird*, however, lacks the angular resolution needed to make significant contributions to other key science objectives. The US *EPIC-CS* mission is the most similar to the present proposal but has considerably less frequency coverage, fewer frequency bands, and no absolute spectral capability. The US mission concept *PIXIE* proposes an improved version of the *FIRAS* spectrometer to measure B-modes and perform absolute spectroscopy simultaneously, but with an effective resolution of only  $2.6^\circ$ .

**Cluster observations:** When *PRISM* flies, the *eROSITA* X-ray survey will likely be the only deeper all-sky cluster survey available. 20–30 times more sensitive than ROSAT, *eROSITA*'s principal goal is to explore cosmological models using galaxy clusters. Forecasts predict that *eROSITA* will detect  $\sim 10^5$  clusters at more than 100 photon counts, which is sufficient to provide a good detection and in many cases to detect the source as extended in X-rays. The main survey provides a good sample of galaxy clusters typically out to  $z = 1$  with some very massive and exceptional clusters at larger distance.

The large majority of these clusters will be re-detected by *PRISM* and thus provide an invaluable inter-calibration of X-ray and SZ effect cluster cosmology, provide determinations of cluster temperatures by combining the two detection techniques, and obtain independent cluster distances for many thousands of clusters whose X-ray temperatures and shape parameters can be obtained from the X-ray survey. With  $\sim 10^6$  clusters detected with *PRISM*, one can further exploit the *eROSITA* survey data by stacking in a way similar to the analysis of the X-ray signals from the ROSAT All-Sky Survey for SDSS detected clusters (Rykoff et al. 2008).

**Other sub-millimeter/far-infrared initiatives:** Existing (*APEX*, *ASTE*, *IRAM 30m*, *LMT*) and future (*CCAT*) ground-based single-dish submillimeter observatories are not as sensitive above 300 GHz as *PRISM*, mainly because of the limitations of observing through the atmosphere. Interferometers (*ALMA*, *CARMA*, *PdB Interferometer*, *SMA*) are ill-suited to observing large fields. Moreover most interferometers are insensitive to large-scale structure. *SKA* will span the radio range from 0.07 GHz up to 20 GHz, and will be the perfect complement to *PRISM*, with more than  $10^9 (f_{sky}/0.5)$  HI galaxies in a redshift range  $0 < z < 1.5$ , and maps of the epoch of reionization above  $z \sim 6$ .

*PRISM* will map the full-sky, large-scale continuum emission at higher sensitivities than ground based single-dish telescopes. Bright compact sources found by *PRISM* in its all-sky surveys can subsequently be observed in more detail by interferometers. Observations can be combined to produce superior maps of selected sky regions. The Atacama Large Millimeter Array (*ALMA*), operating in the range 30-1000 GHz, will complement *PRISM* with follow-up of sources and clusters detected by *PRISM*, mapping their structure in total intensity, polarization and spectral line at high angular and spectral resolution.

*CCAT* will initially have two imaging instruments. At low frequencies, *LWCam* on *CCAT* will be able to detect sources below the *PRISM* confusion limit relatively quickly. However variations in atmospheric transmissivity and thermal radiation from the atmosphere make it difficult for *CCAT* to map large scale structures. At high frequencies, *SWCam* will have difficulty mapping large areas to the confusion limit of *PRISM*. Based on the specifications from Stacey et al. (2013), *CCAT* can map an area of 1 square degree at 857 GHz to a sensitivity of 6 mJy (the *PRISM* confusion limit) within 1 hour. To map the entire southern sky to this same depth requires  $\sim 900$  days (24h) with optimal observing conditions. Such large scale observations will not be feasible with *CCAT*. *PRISM* is needed to produce all-sky maps in these frequency bands. *PRISM* will produce maps at the same resolution as *Herschel*. However *Herschel* was able to map only a limited portion of the sky.

Few previous infrared telescopes have performed all-sky surveys in the bands covered by *PRISM*. *Akari* was the last telescope to perform such observations, but the data is at much lower sensitivity and resolution and is not yet publicly available. Several other prior telescopes (*Spitzer*, *Herschel*) as well as the airborne observatory *SOFIA* and the future mission *SPICA* have observed or will observe in the 600-4000 GHz range, but only over very limited areas of the sky. Furthermore, except for a few deep fields, they observe objects already identified in other bands. *PRISM* will be able to perform observations with sensitivities comparable to *Herschel* or better, but covering the entire sky in many frequency bands.

## References

- [1] A. Avgoustidis, E.J. Copeland, A. Moss, et al. *Phys.Rev.Lett.*, 107:121301, 2011.
- [2] R. Barkana and A. Loeb. *Phys. Repts.*, 349:125-238, 2001.
- [3] J. D. Barrow and P. Coles. *MNRAS*, 248:52-57, 1991.
- [4] J. G. Bartlett and J. Silk. *ApJ*, 353:399-405, 1990.
- [5] K. Basu, C. Hernández-Monteagudo, and R. A. Sunyaev. *A&A*, 416:447-466, 2004.
- [6] D. Baumann et al. *AIP Conf.Proc.*, 1141:10-120, 2009.
- [7] C. L. Bennett, M. Halpern, G. Hinshaw, et al. *ApJS*, 148:1-27, 2003.
- [8] M. Birkinshaw. *Phys. Rep.*, 310:97-195, 1999.
- [9] F.R. Bouchet et al. *arXiv:1102.2181*, 2011.
- [10] P. Bull and M. Kamionkowski. *ArXiv:1302.1617*, 2013.
- [11] C. Burigana. In G. L. Chincarini, A. Iovino, T. Maccacaro, & D. Maccagni, editor, *Observational Cosmology*, volume 51 of *Astronomical Society of the Pacific Conference Series*, 1993.
- [12] C. Burigana, L. Danese, and G. de Zotti. *A&A*, 246:49-58, 1991.
- [13] B. J. Carr, K. Kohri, Y. Sendouda, and J. Yokoyama. *Phys.Rev.D*, 81:104019, 2010.
- [14] R. Cen and J. P. Ostriker. *ApJ*, 514:1-6, 1999.
- [15] A. Challinor and A. Lasenby. *ApJ*, 499:1, 1998.
- [16] J. Chluba. *Spectral Distortions of the Cosmic Microwave Background*. PhD thesis, LMU München, 2005.
- [17] J. Chluba. *MNRAS*, 402:1195-1207, 2010.
- [18] J. Chluba. *ArXiv:1304.6120*, 2013.
- [19] J. Chluba. *ArXiv e-prints: 1304.6121*, 2013.
- [20] J. Chluba and D. Grin. *ArXiv:1304.4596*, 2013.
- [21] J. Chluba and R. A. Sunyaev. *A&A*, 458:L29-L32, 2006.
- [22] J. Chluba and R. A. Sunyaev. *MNRAS*, 419:1294-1314, 2012.
- [23] J Chluba, A Erickcek, and I Ben-Dayan. *Ap.J.*, 758:76, 2012.
- [24] J. Chluba, A. L. Erickcek, and I. Ben-Dayan. *ApJ*, 758:76, 2012.
- [25] J. Chluba, R. Khatri, and R. A. Sunyaev. *MNRAS*, 425:1129-1169, 2012.
- [26] S. Chongchitnan and G. Efstathiou. *Phys.Rev.D*, 72:083520, 2005.
- [27] R. M. Crutcher. *ARA&A*, 50:29-63, 2012.
- [28] R. A. Daly. *ApJ*, 371:14-28, 1991.
- [29] L. Danese and C. Burigana. In J. L. Sanz, E. Martinez-Gonzalez, and L. Cayon, editors, *Present and Future of the Cosmic Microwave Background*, volume 429 of *Lecture Notes in Physics*, Berlin Springer Verlag, 1994.
- [30] L. Danese and G. de Zotti. *Nuovo Cimento Rivista Serie*, 7:277-362, 1977.
- [31] J. B. Dent, D. A. Easson, and H. Tashiro. *Phys.Rev.D*, 86:023514, 2012.
- [32] B. T. Draine. In T. Henning, E. Grün, and J. Steinacker, editors, *Cosmic dust: Near and far*, volume 414 of *Astronomical Society of the Pacific Conference Series*, 2009.
- [33] B. T. Draine and B. Hensley. *ApJ*, 765:159, 2013.
- [34] V. K. Dubrovich. *Sov. Ast. Lett.*, 1:196, 1975.
- [35] J. L. Feng. *ARA&A*, 48:495, 2010.
- [36] J. L. Feng, A. Rajaraman, and F. Takayama. *Phys.Rev.D*, 68:063504, 2003.
- [37] D. J. Fixsen, E. S. Cheng, J. M. Gales, et al. *ApJ*, 473:576, 1996.
- [38] J. Ganc and E. Komatsu. *Phys.Rev.D*, 86:023518, 2012.
- [39] J Ganc and E Komatsu. *Phys.Rev.*, D86:023518, 2012.
- [40] P. Goldreich and N. D. Kylafis. *ApJL*, 243:L75-L78, 1981.
- [41] Y. Gong, A. Cooray, M. Silva, et al. *ApJ*, 745:49, 2012.
- [42] M. J. Griffin et al. *A&A*, 518:L3, 2010.
- [43] A. C. Hall and A. Challinor. *MNRAS*, 425:1170-1184, 2012.
- [44] P. Hennebelle and E. Falgarone. *A&A Rev.*, 20:55, 2012.
- [45] C. Hernández-Monteagudo and R. A. Sunyaev. *MNRAS*, 359:597-606, 2005.
- [46] C. Hernández-Monteagudo, L. Verde, and R. Jimenez. *ApJ*, 653:1-10, 2006.
- [47] C. Hernández-Monteagudo, Z. Haiman, R. Jimenez, and L. Verde. *ApJL*, 660:L85-L88, 2007.
- [48] C. Hernández-Monteagudo, J. A. Rubiño-Martín, and R. A. Sunyaev. *MNRAS*, 380:1656-1668, 2007.
- [49] W. Hu and J. Silk. *Phys.Rev.D*, 48:485-502, 1993.
- [50] W. Hu and J. Silk. *Phys. Rev. Lett.*, 70:2661, 1993.
- [51] W. Hu and N. Sugiyama. *ApJ*, 436:456-466, 1994.
- [52] W. Hu, D. Scott, and J. Silk. *ApJL*, 430:L5-L8, 1994.
- [53] W. Hu, D. Scott, and J. Silk. *Phys.Rev.D*, 49:648-670, 1994.
- [54] A. F. Illarionov and R. A. Sunyaev. *Astronomicheskii Zhurnal*, 51:1162-1176, 1974.
- [55] N. Itoh, Y. Kohyama, and S. Nozawa. *ApJ*, 502:7, 1998.
- [56] R. J. Ivison, A. M. Swinbank, I. Smail, et al. *ArXiv e-prints:1302.4436*, 2013.
- [57] K. Jedamzik, V. Katalinić, and A. V. Olinto. *Physical Review Letters*, 85:700-703, 2000.
- [58] R. Khatri and R. A. Sunyaev. *JCAP*, 6:038, 2012.
- [59] R. Khatri and R. A. Sunyaev. *JCAP*, 9:016, 2012.
- [60] R. Khatri and R. A. Sunyaev. *ArXiv:1303.7212*, 2013.
- [61] R. Khatri, R. A. Sunyaev, and J. Chluba. *A&A*, 540:A124, 2012.
- [62] R. Khatri, R. A. Sunyaev, and J. Chluba. *A&A*, 543:A136, 2012.
- [63] W. H. Kinney. *Phys.Rev.D*, 66:083508, 2002.
- [64] L. Kuzmin, G. Yassin, S. Withington, and P. Grimes. In A. Karpov, editor, *Eighteenth International Symposium on Space Terahertz Technology*, 2007.
- [65] A. Lapi, J. González-Nuevo, L. Fan, et al. *ApJ*, 742:24, 2011.
- [66] A. Lewis, J. Weller, and R. Battye. *MNRAS*, 373:561-570, 2006.
- [67] K. Lochan, S. Das, and A. Bassi. *Phys.Rev.D*, 86:065016, 2012.
- [68] J. C. Mather, E. S. Cheng, D. A. Cottingham, et al. *ApJ*, 420:439-444, 1994.
- [69] P. McDonald, R. J. Scherrer, and T. P. Walker. *Phys.Rev.D*, 63:023001, 2001.

- [70] J.-B. Melin, J. G. Bartlett, and J. Delabrouille. *A&A*, 459:341-352, 2006.
- [71] F. Miniati, D. Ryu, H. Kang, et al. *ApJ*, 542:608-621, 2000.
- [72] M. Negrello, R. Hopwood, G. De Zotti, et al. *Science*, 330:800, 2010.
- [73] S. P. Oh, A. Cooray, and M. Kamionkowski. *MNRAS*, 342:L20-L24, 2003.
- [74] J. P. Ostriker and C. Thompson. *ApJL*, 323:L97-L101, 1987.
- [75] E. Pajer and M. Zaldarriaga. *Phys. Revs. Lett.*, 109:021302, 2012.
- [76] E. Pajer and M. Zaldarriaga. *Phys.Rev.Lett.*, 109:021302, 2012.
- [77] H. V. Peiris, E. Komatsu, L. Verde, et al. *ApJS*, 148:213-231, 2003.
- [78] J. L. Pineda, W. D. Langer, T. Velusamy, and P. F. Goldsmith. *ArXiv e-prints*, 2013.
- [79] Planck Collaboration, N. Aghanim, M. Arnaud, et al. *A&A*, 536:A12, 2011.
- [80] Planck Collaboration, P. A. R. Ade, N. Aghanim, et al. *ArXiv e-prints:1212.4131*, 2012.
- [81] Planck Collaboration, P. A. R. Ade, N. Aghanim, et al. *ArXiv e-prints:1303.5077*, 2013.
- [82] Planck Collaboration, P. A. R. Ade, N. Aghanim, et al. *ArXiv e-prints:1303.5085*, 2013.
- [83] Planck Collaboration, P. A. R. Ade, N. Aghanim, et al. *ArXiv:1303.5084*, 2013.
- [84] Planck Collaboration, P. A. R. Ade, N. Aghanim, et al. *ArXiv:1303.5076*, 2013.
- [85] Planck Collaboration, P. A. R. Ade, N. Aghanim, et al. *ArXiv:1303.5081*, 2013.
- [86] Planck Collaboration XXII. *arXiv:1303.5082*, 2013.
- [87] P. P. Ponente, J. M. Diego, R. K. Sheth, et al. *MNRAS*, 410:2353-2362, 2011.
- [88] B. A. Powell. *ArXiv:1209.2024*, 2012.
- [89] Y. Rephaeli. *ApJ*, 445:33-36, 1995.
- [90] Y. Rephaeli and O. Lahav. *ApJ*, 372:21-24, 1991.
- [91] D. A. Riechers, C. M. Bradford, D. L. Clements, et al. *Nature*, 496:329-333, 2013.
- [92] J. A. Rubiño-Martín, C. Hernández-Monteagudo, and R. A. Sunyaev. *A&A*, 438:461-473, 2005.
- [93] J. A. Rubiño-Martín, J. Chluba, and R. A. Sunyaev. *MNRAS*, 371:1939-1952, (RMCS06), 2006.
- [94] J. A. Rubiño-Martín, J. Chluba, and R. A. Sunyaev. *A&A*, 485:377-393, 2008.
- [95] S. Y. Sazonov and R. A. Sunyaev. *ApJ*, 508:1-5, 1998.
- [96] U. Seljak and M. Zaldarriaga. *ApJ*, 538:57-64, 2000.
- [97] J. Smidt, A. Amblard, C. T. Byrnes, et al. *Phys.Rev.D*, 81(12):123007, 2010.
- [98] K.M. Smith, A. Cooray, S. Das, et al. *AIP Conference Proceedings*, 1141:121, 2009.
- [99] R. A. Sunyaev and J. Chluba. *Astronomische Nachrichten*, 330:657, 2009.
- [100] R. A. Sunyaev and Y. B. Zeldovich. *Astrophysics and Space Science*, 9:368-382, 1970.
- [101] R. A. Sunyaev and Y. B. Zeldovich. *A&A*, 20:189, 1972.
- [102] R. A. Sunyaev and Y. B. Zeldovich. *Comments on Astrophysics and Space Physics*, 4:173, 1972.
- [103] H. Tashiro, E. Sabancilar, and T. Vachaspati. *Phys.Rev.D*, 85:103522, 2012.
- [104] H. Tashiro, E. Sabancilar, and T. Vachaspati. *ArXiv:1212.3283*, 2012.
- [105] Planck HFI Core Team. *A&A*, 536:A4, 2011.
- [106] T. Treu. *ARA&A*, 48:87-125, 2010.
- [107] L Verde, H Peiris, and R Jimenez. *JCAP*, 0601:019, 2006.
- [108] Y. B. Zeldovich and R. A. Sunyaev. *Astrophysics and Space Science*, 4:301-316, 1969.
- [109] P. Zhang, U.-L. Pen, and H. Trac. *MNRAS*, 355:451-460, 2004.